Check for updates

View Article Online
View Journal

Dalton Transactions

Accepted Manuscript

This article can be cited before page numbers have been issued, to do this please use: A. L. Amorim, M. M. Peterle, A. Guerreiro, D. F. Coimbra, R. S. Heying, G. F. Caramori, A. L. Braga, A. J. Bortoluzzi, A. Neves, G. J. L. Bernardes and R. Peralta, *Dalton Trans.*, 2019, DOI: 10.1039/C9DT00616H.

This is an Accepted Manuscript, which has been through the Royal Society of Chemistry peer review process and has been accepted for publication.

Accepted Manuscripts are published online shortly after acceptance, before technical editing, formatting and proof reading. Using this free service, authors can make their results available to the community, in citable form, before we publish the edited article. We will replace this Accepted Manuscript with the edited and formatted Advance Article as soon as it is available.

You can find more information about Accepted Manuscripts in the author guidelines.

Please note that technical editing may introduce minor changes to the text and/or graphics, which may alter content. The journal's standard Terms & Conditions and the ethical guidelines, outlined in our author and reviewer resource centre, still apply. In no event shall the Royal Society of Chemistry be held responsible for any errors or omissions in this Accepted Manuscript or any consequences arising from the use of any information it contains.

ROYAL SOCIETY OF CHEMISTRY

rsc.li/dalton

Dalton Transactions

View Article Online
DOI: 10.1039/C9DT00616H

ARTICLE

Synthesis, Characterization and Biological Evaluation of New Manganese Metal Carbonyl Compounds That Contain Sulfur and Selenium Ligands as a Promising New Class of CORMs

Received 00th January 2019,
Accepted 00th January 20xx

DOI: 10.1039/x0xx00000x

www.rsc.org/

André L. Amorim,[a,§] Marcos M. Peterle,[a,§] Ana Guerreiro,[b] Daniel F. Coimbra,[a] Renata S. Heying,[a] Giovani F. Caramori,[a] Antonio L. Braga,*[a] Adailton J. Bortoluzzi,[a] Ademir Neves,[a] Gonçalo J. L. Bernardes[b,c] and Rosely A. Peralta*[a]

Three new manganese carbonyl compounds with heavy atom donors were synthesized and their potential use as photoCORMS was evaluated. Interestingly, all compounds had an elusive binding mode, in which the ligands adopted a κ^2-X coordination (where X = S or Se), confirmed both by X-ray crystallography and IR spectroscopy. The stability of the title compounds in the dark was determined by monitoring the changes in the UV spectra of the compounds in both dichloromethane and acetonitrile. These studies show that in coordinating solvents there is an exchange of the bromide bonded to the metal centre by a solvent molecule, which is evidenced by the changes in the UV and IR spectra and by DFT analysis. EDA and natural bond order analyses were conducted to evaluate the influence of the heavy atom donors in the first coordination sphere of the compounds. Photoexcitation at 380 nm demonstrated that all compounds showed release of all three COs, as seen in the photoproducts detected by IR spectroscopy. Furthermore, CO release was observed when the photoCORMs were incubated with living cells, and we observed a CO-dependent inhibition of cell viability.

Introduction

Since the discovery of the signalling properties of carbon monoxide[1,2] and its potential use as a therapeutic agent,[3-5] several research groups have begun to study ways to deliver CO in a safe manner and limit the hazards.[6] One way to limit its cytotoxicity is to use carbon monoxide-releasing molecules (CORMs)[7,8] for which the release of CO is prompted by the use of an external trigger,[9] such as photoexcitation. This is one of the most commonly employed procedures that gave rise to so-called photoCORMs.[10] Even though some organic CO carriers have been developed,[11-18] metal carbonyl compounds (MCCs)[8] are still common because of the diverse array of properties associated with the metal centre,[9] which lead to the development of ruthenium, iron, rhenium, molybdenum and manganese MCCs,[19-23] the latter being of the most common.

Currently, a wide list of examples of manganese MCCs with either different ligands or dinuclear species, which can help in the design of new photoCORMs, can be found in the literature, such as L^1-k^2N^1,N^2 (2,6-bis(benzimidazole-2'-yl)pyridine),[24] pyTAm (2-(pyridyl)imino-triazaadamantane)[25] and the dinuclear rhenium-manganese carbonyl.[26] These photoCORMs have different applications concerning their biological stability, photoswitch probes upon CO release and visible light activation. In general, these compounds have Mn^I centres with either bidentate or facial tridentate ligands. However, it has been shown that the use of ligands with nonbonding groups, such as tris(2-pyridylmethyl)amine (tpa), which adopts a κ^3 binding mode, can facilitate the formation of inactivated CORMS (iCORMs) after the CO-release procedure.[27] After the dissociation, either the released CO molecules are substituted by a species present in the medium, typically a solvent molecule, or the ligand suffers dissociation of the metal framework, and the use of switch on probes, such as imdansyl can help elucidate this mechanism and provide an insight into the localization of the CO prodrug.[28] Despite these recent advances, most manganese photoCORMs have CO-release activity only near the UV region, which limits their applicability. In this context, the use of ligands that can shift the excitation bands towards lower energy, such as bis(4-chloro-phenylimino)acenaphthene and azopyridines,[29,30] are highly desirable.

Although various examples of new and interesting ligands can be found in the literature, the use of heavy atoms in the ligand framework has not been reported. In this regard, the increase in the spin-orbit coupling (SOC) with the use of heavier atoms, such as sulfur and selenium, can modify the CO dissociation and increase the intersystem crossing (ISC) between singlet and triplet excited states.[31]

Herein, we focus on the design of new ligands that contain heavy atoms in the ligand framework of manganese photoCORMs that could potentially modify the photoexcitation

[a] Departamento de Química, Universidade Federal de Santa Catarina, Florianópolis, Santa Catarina 88040-900, Brazil.
[b] Instituto de Medicina Molecular, Faculdade de Medicina, Universidade de Lisboa, Avenida Professor Egas Moniz, 1649-028, Lisboa (Portugal).
[c] Department of Chemistry, University of Cambridge, Lensfield Road, Cambridge CB2 1EW (UK)
*E-mail: rosely.peralta@ufsc.br; Tel: +55(48)3721 3627
Email: Braga.antonio@ufsc.br

†Electronic Supplementary Information (ESI) available free of charge: See DOI: 10.1039/x0xx00000x.

‡Crystallographic information available free of charge at the Cambridge Crystallographic Data Centre as supplementary publication numbers CCDC 1894674, 1894675 and 1894677.

§Both authors contributed equally to this work.

Published on 28 March 2019. Downloaded on 3/29/2019 1:23:54 AM.

Dalton Transactions Accepted Manuscript

View Article Online
DOI: 10.1039/C9DT00616H

Published on 28 March 2019. Downloaded on 3/29/2019 1:23:54 AM.

behaviour of these compounds. For this purpose, three chalcogen-containing ligands and their respective MCCs were synthesized (Figure 1), phS (**1'**), phSe (**2'**), bzlSe (**3'**), [$MnBr(CO)_3$(phS-κ^2 S)] (**1**), [$MnBr(CO)_3$(phSe-κ^2 Se)] (**2**) and [$MnBr(CO)_3$(bzlSe-κ^2 Se)] (**3**) and their properties were evaluated by common characterization techniques and theoretical approaches.

Results and discussion

Ligands **1'–3'** were synthesized by the reaction of bis(2-chloroehtyl)amine hydrochloride with the appropriate selenolate or thiolate, which were generated in situ by the cleavage of the selected dichalcogenide with sodium borohydride. The products were purified by column chromatography and obtained in good yields. The ligands were characterized by IR, ^{1}H, ^{13}C and ^{77}Se NMR spectroscopy (Figures S1–S11).[32]

The manganese metal carbonyl compounds were synthesized by heating at reflux a 4:1 diethyl ether/acetonitrile mixture of ligands and $Mn(CO)_5Br$ precursor in dim light conditions overnight, similar to already published procedures.[33] Slow diffusion of hexane into the solutions led to the formation of yellow to orange crystals, which were collected and kept under an argon atmosphere at –20°C and used for characterization.

Solid-state characterization

The attenuated total reflectance (ATR) IR spectra for compounds **1–3** showed three intense bands at around 2050 and 1850 cm^{-1}, attributed to the CO stretching frequencies. This is consistent with a facial orientation of the carbonyl groups and a distorted C_{3v} symmetry (Figures S12–S14). The higher energy frequency, centred at 2020, 2015 and 2015 cm^{-1} for **1**, **2** and **3**, respectively, is attributed to symmetric CO stretching whereas the lower frequency energies centred at 1933/1912, 1919/1896 and 1927/1908 cm^{-1} are originated from a split in the antisymmetric CO stretching band. In general, manganese tricarbonyl compounds with tridentate symmetric ligands form compounds with facial bonded ligands and a much less degenerate unsymmetric stretching band. This splitting indicates that the ligands of the compounds synthesized are bonded in a bidentate fashion with no displacement of the bromide from the first coordination sphere. The splitting of the degenerate band, a direct comparison of the bands for compounds **1** and **2**, which are structurally similar, also reveals that the use of heavier and softer ligands shifts the CO stretching frequencies to lower energy. This indicates an increase in the metal to ligand charge transfer (MLCT) that increases the C–O bond length with heavier atoms. Analysis with other manganese MCCs, such as $[Mn(CO)_3$(tpa-k^3 N)]Br[27] (with ν_{CO}: 2032, 1961 and 1905 cm^{-1}) and CORM-ONN1[33] (with ν_{CO}: 2040, 1941, 1920 cm^{-1}), reinforces this finding.

The above statement is corroborated by the crystal data obtained for compounds **1–3**. In all three cases, the ligand binds in a bidentate mode to form a five-membered ring. The use of mild synthetic conditions with diethyl ether as the solvent did not favour the displacement of the bromide present in the starting material, and one of the sulfur or selenium moieties remained uncoordinated.

The crystallographic parameters are summarized in Table S1–S6 and the relevant bond lengths and angles are displayed in Table 1, and show that the *trans* influence takes place, which influences the Mn–C bond lengths. The use of softer ligands shortens the Mn–C bond *trans* to the soft moiety, with the Mn–C bonds *trans* to the bromide being slightly more compressed. As a direct consequence, all three Mn–C bonds differ in some way, deviating from the C_{3v} symmetry, which is consistent with the non-degenerate character of the CO antisymmetric stretching seen in the IR spectra. As expected, the softer binding moieties, sulfur and selenium, have a much higher M–X (where X = S or Se) bond length relative to typical nitrogen ligands, due to their higher covalent radii. The remainder of the bond lengths and angles are within typical ranges considering previously published manganese tricarbonyl compounds.[34,35] The molecular structures for **1–3** are represented in Figure 2.

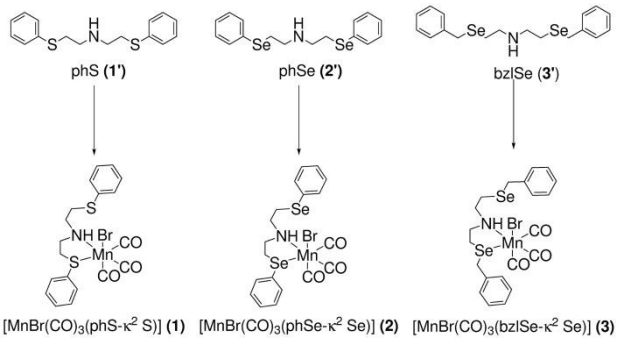

Figure 1 Structural representation of the ligands phS (**1'**), phSe (**2'**), bzlSe (**3'**) and their respective manganese carbonyl compounds used in this study, from left to right: [$MnBr(CO)_3$(phS-κ^2 S)] (**1**), [$MnBr(CO)_3$(phSe-κ^2 Se)] (**2**) and [$MnBr(CO)_3$(bzlSe-κ^2 Se)] (**3**).

Table 1 Selected bond lengths (Å) and angles (°) for **1–3**.

	1	2	3
Bonds			
Mn1-C1	1.810(3)	1.803(4)	1.817(5)
C1-O1	1.142(3)	1.145(5)	1.140(6)
Mn1-C2	1.804(3)	1.801(4)	1.806(5)
C2-O2	1.142(3)	1.149(5)	1.141(6)
Mn1-C3	1.795(3)	1.790(4)	1.788(5)
C3-O3	1.143(3)	1.148(5)	1.138(6)
Mn1-N1	2.1255(19)	2.131(3)	2.129(4)
Mn1-S2	2.3748(6)	-	-
Mn1-Se1	-	-	2.4625(8)
Mn1-Se2	-	2.4758(7)	-
Mn1-Br1	2.5288(4)	2.5280(6)	2.5344(8)
Angles			
C1-Mn1-C2	88.43(12)	88.39(19)	88.0(2)
C1-Mn1-C3	91.21(12)	90.73(18)	92.2(2)
C2-Mn1-C3	90.67(11)	90.70(18)	92.1(2)
N1-Mn1-S2	85.05(5)	-	-
N1-Mn1-Se1	-	-	85.11(11)
N1-Mn1-Se2	-	85.96(8)	-
S2-Mn1-Br1	83.918(18)	-	-
Se1-Mn1-Br1	-	-	82.47(3)
Se2-Mn1-Br1	-	82.49(2)	-

Dalton Transactions Accepted Manuscript

This journal is © The Royal Society of Chemistry 2019

Please do not adjust margins

View Article Online
DOI: 10.1039/C9DT00616H

Published on 28 March 2019. Downloaded on 3/29/2019 1:23:54 AM.

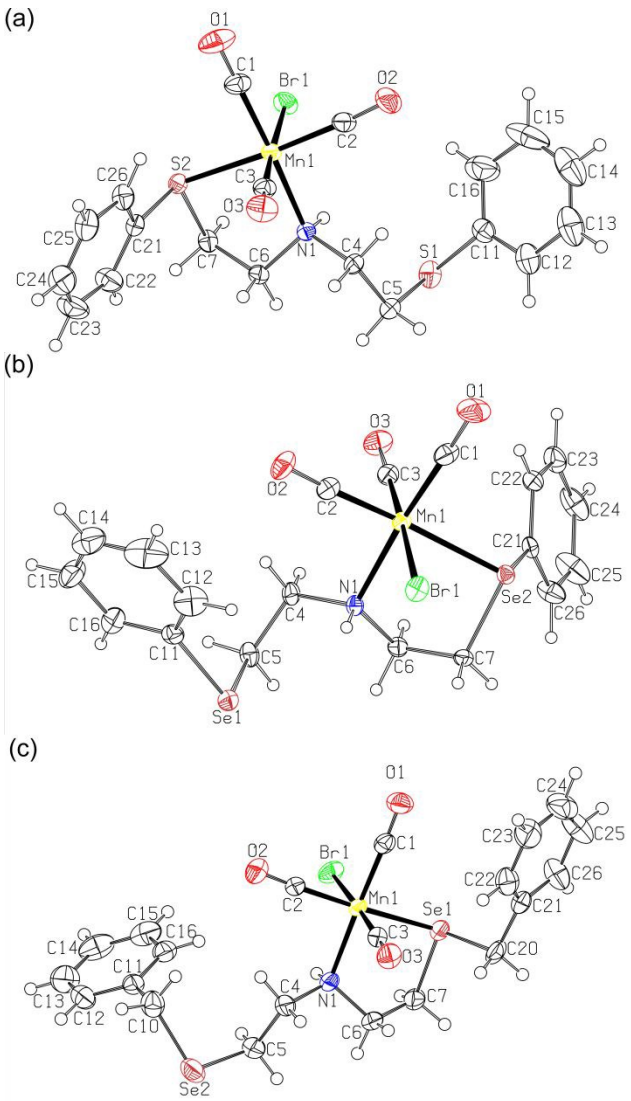

Figure 2 Molecular structures of compounds **1–3**, ellipsoids with 40% probability. a) [MnBr(CO)$_3$(phS-κ^2 S)]; b) [MnBr(CO)$_3$(phSe-κ^2 Se)], and c) [MnBr(CO)$_3$(bzlSe-κ^2 Se)].

Bonding Analysis

The Mn–CO bonding situations were analysed in the light of both Kohn-Sham energy decomposition analysis (GKS-EDA) and natural bond orbital (NBO) analyses. The GKS-EDA quantifies the bonding strength and decomposes it on several meaningful terms to reveal that in compounds **1–3** the carbonyl group coordinated trans to bromide ion, C3O3, interacts more strongly with the Mn1 centre than the two other carbonyl groups, C1O1 and C2O2, which are coordinated trans to nitrogen and chalcogen atoms (S or Se), respectively (Table 2). The total binding energy values for Mn1-C3O3 vary from –54.06 to –58.05 kcal mol^{-1}, whereas for Mn1-C1O1 and Mn1-C2O2 they vary from –41.97 to –47.27 kcal mol^{-1}. In fact, the total interaction energy values (ΔE^{int}) shows that, in all cases, the C2O2 group is the most labile one (–41.97– –42.61 kcal mol^{-1}). Such findings are totally in line with the solid-state characterization, which reveals the three Mn-CO bonds are different as a consequence of the trans effect. Such effect is also confirmed by means of the GKS-EDA terms.

Table 2 Energy Decomposition Analysis (GKS-EDA) of M–CO bonds (kcal.mol^{-1}) at BP86-D3/def2-SVP level of theory.

Interaction	ΔE^{int}	ΔE^{elstat}	ΔE^{exch}	ΔE^{rep}	ΔE^{pol}	ΔE^{disp}	ΔE^{corr}
			1				
Mn1-C1O1	-46.31	-146.59	-225.04	465.74	-94.69	-2.54	-43.19
Mn1-C2O2	-41.97	-148.37	-229.74	477.28	-97.59	-4.38	-39.15
Mn1-C3O3	-54.06	-148.92	-228.06	471.95	-98.41	-4.68	-45.93
			2				
Mn1-C1O1	-47.27	-146.80	-225.38	466.28	-94.63	-2.40	-44.34
Mn1-C2O2	-42.61	-151.31	-233.43	486.30	-101.16	-4.51	-38.50
Mn1-C3O3	-54.98	-148.96	-228.95	473.05	-98.27	-4.82	-47.04
			3				
Mn1-C1O1	-46.71	-143.01	-218.82	452.53	-90.58	-3.04	-43.79
Mn1-C2O2	-42.43	-152.79	-236.94	492.90	-103.84	-3.99	-37.77
Mn1-C3O3	-58.05	-149.55	-232.21	478.38	-101.21	-5.28	-48.18

The nature of the chalcogen employed has a remarkable effect on the Mn1-C2O2 and Mn1-C3O3 bonding situations. For instance, on going from **1** to **2**, it can be noticed that the electrostatic, ΔE^{elstat}, exchange, ΔE^{exch}, and polarization, ΔE^{pol}, contributions for Mn1-C2O2 become more stabilizing, suggesting an increase of the electronic charge reorganization, including charge transfer and polarization. A similar situation, but with slight magnitude is also observed for Mn1-C3O3 (Table 2). By changing the ligand (phSe) to (bzlSe), that means going from **2** to **3**, it is noticed that Mn1-C3O3 becomes still stronger, whereas the two other Mn–CO bonds are slightly less strong. In fact, the GKS-EDA results reveal that both the nature of the chalcogen as well as the ligand employed have non-negligible and distinguishable electronic effects on the Mn–CO bonding situations. The Wiberg bond indexes and natural population analysis (NPA) obtained from natural bond order method, a localized form of the molecular wavefunction also confirms the differences on Mn-CO bond lengths as well as the electronic charge reorganization (Table S10).

Identification of the active species in solution

Because the isolated compounds show the ligands binding in a bidentate mode with a bromide in the first coordination sphere, it is reasonable to expect that the absorption bands on the UV spectra for these compounds will show solvent-dependent behaviour, with the exchange of the bromide present in the first coordination sphere for a coordinating solvent. Thus, the UV spectra for **1–3** were analysed under two conditions: a nonbonding and a bonding solvent, namely dichloromethane and acetonitrile, respectively.

In dichloromethane, compounds **1, 2** and **3** present broad absorption bands with λ_{max} at 385 nm (2597 mol L^{-1} mol^{-1}), 385 nm (2235 mol L^{-1} mol^{-1}) and 388 nm (2014 mol L^{-1} mol^{-1}), respectively. Because these bands did not show any sign of modification over a 24h incubation period in the dark (Figure 3 for **3** and S15–S16), the structures must retain the bidentate binding mode [MnBr(CO)$_3$(L-κ^2 X)] (in which L = phS, phSe or bzlSe and X = S or Se).

Dalton Transactions Accepted Manuscript

Please do not adjust margins

View Article Online
DOI: 10.1039/C9DT00626H

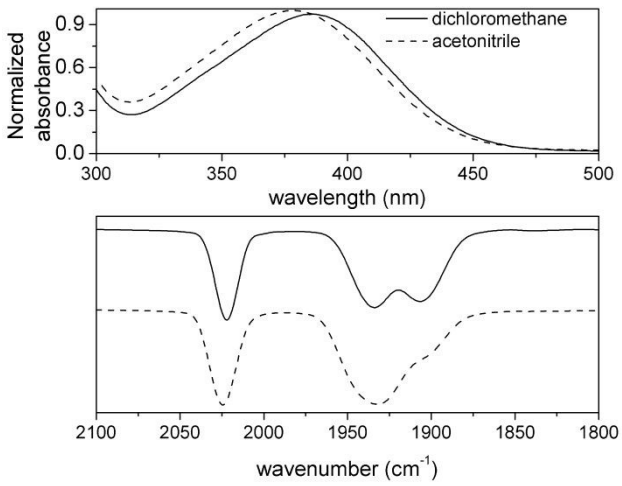

Figure 3 UV (top) and IR (bottom) spectral changes of **2** over 24 h period in the dark in dichloromethane (top) and acetonitrile (bottom).

It was also possible to analyse the stability of **1–3** in dichloromethane over the course of the incubation period by IR spectroscopy, which showed that the three CO stretching bands remain unchanged, both in terms of their energy and their intensity during analysis (Figure 3 for **2** and S17–S18). Interestingly, a direct comparison between the solid ATR and the diluted solution in KBr is not possible because the stretching frequencies for the sample in KBr pellets are shifted towards higher energy, ≈10 and 20 cm^{-1} for the symmetric and antisymmetric stretching modes, respectively. The frequencies for the L-κ^2 binding modes are summarized in Table 3. This difference observed for the solid ATR and the diluted solution in KBr is due to the presence of intermolecular forces between the sample and some of the water present in the KBr pellets.

With addition of acetonitrile the spectral profile slowly changes, with the absorption bands shifting to higher energy (Figure 3 for **2** and S15–S16). Over the same 24h period in a 1:1 dichloromethane/acetonitrile the bands are hypsochromically shifted by 20 nm, with λ_{max} at 365, 365 and 368 nm, respectively. These shifts could indicate that there is a displacement of the bonded bromide by acetonitrile, which would result in the formation of $[Mn(CH_3CN)(CO)_3(L\text{-}\kappa^2\ X)]^+$ species (in which L = phS, phSe or bzlSe and X = S or Se). Further displacement of the solvent molecule by the pendant moiety to form $Mn(CO)_3(L\text{-}\kappa^3)]^+$ was not detected over the course of the experiment, since no red shift of the initial absorption bands due to the coordination of the pendant moiety are detected.

To elucidate if there is a ligand exchange between the bromide and a solvent molecule, the IR spectra were also obtained for the species formed during the incubation periods. In this media the three stretching bands shows minor shifts to lower energies, and the nondegenerate character of the antisymmetric stretching band is maintained for all three compounds. This behaviour indicates that the distorted C_{3v} character is maintained, without exchange of the bromide by a solvent molecule, which would shift the CO stretching to higher frequencies, nor the coordination of the pendant moiety to the metal centre, , which would increase the degeneracy of the bands, similar behaviour is already reported in the literature.[36]

Table 3 Experimental and calculated carbonyl stretching frequencies for the manganese carbonyl compounds used in this study in both solvents (in which X = S or Se) at BP86-D3/def2-SVP level of theory.

Ligand (L)	phS		phSe		bzlSe	
	$[MnBr(CO)_3L\text{-}\kappa^2\ X]$					
	exp	calc	exp	calc	exp	Calc
symmetric	2027	2014	2022	2010	2024	2012
antisymmetric	1938	1932	1934	1928	1934	1929
	1917	1904	1906	1899	1916	1883
	$[Mn(CH_3CN)(CO)_3L\text{-}\kappa^2\ X]^+$					
	exp		exp		Exp	
symmetric	2023		2024		2023	
antisymmetric	1924		1932		1932	
	1900		1898		1911	

The changes in the CO stretching bands are shown in Figure 3 for **2** (S17–S18 for **1** and **3**) and the results displayed in Table 3. Unfortunately, the isolation of the species $[Mn(CH_3CN)(CO)_3(L\text{-}\kappa^2\ X)]^+$ or $[Mn(CO)_3(L\text{-}\kappa^3\ X)]^+$ (in which L = phS, phSe or bzlSe and X = S or Se), which could facilitate the identification of these species, could not be performed.

DFT and TD-DFT analysis of the active species

The $[MnBr(CO)_3(L\text{-}\kappa^2\ X)]$ and $[Mn(CH_3CN)(CO)_3(L\text{-}\kappa^2\ X)]^+$ (in which L = phS, phSe or bzlSe and X = S or Se) binding modes were optimized to gain insight into the geometrical and electronic structures of the species by using density functional theory (DFT) in the gas phase. The absence of imaginary frequencies corroborated the understanding that the optimized structures are truly energy-minimum. These structures were once again optimized to take into account the polarizability of the medium, using the SMD solvation model, with the appropriate solvents.

The calculated frequencies at the BP86-D3/def2-SVP for the $[MnBr(CO)_3(L\text{-}\kappa^2\ X)]$ were compared to the experimental IR frequencies and are in good agreement with the experimental values (Table 3) with deviations in the order of 10 cm^{-1}. The results are consistent with the proposed coordination.

Time-dependent DFT (TD-DFT) calculations were also made. The first forty singlet excited states were calculated for both cases. For $[MnBr(CO)_3(L\text{-}\kappa^2\ X)]$)] (in which L = phS, phSe or bzlSe and X = S or Se) the most prominent band is attributed either to a HOMO-1 → LUMO+1 for phS and phSe ligands and a HOMO-2 → LUMO+1 for the bzlSe ligand, in which for both cases the orbitals comprise mostly manganese *d* orbitals, with some contribution of the bromide p orbitals. The first unoccupied orbitals are π^* orbitals delocalized on the chalcogen and aromatic rings.[37,38] Moreover, the increase in the polarization of the donor did not further displace the MLCT bands to lower energy, even though the LUMO+1 is 0.04 eV lower when going from **1** to **2**, probably due to the higher electrostatic character of the M-X bond when going form S to Se, which is consistent with the EDA results (Figure 4 and Table 4).

As expected, exchanging the solvent from dichloromethane to acetonitrile and exchanging the bromide for acetonitrile, increases the energy of the singlet excitation. Interestingly, for $[Mn(CH_3CN)(CO)_3(L\text{-}\kappa^2\ X)]^+$ compounds the excitations comprise

Published on 28 March 2019. Downloaded on 3/29/2019 1:23:54 AM.

Dalton Transactions Accepted Manuscript

 This journal is © The Royal Society of Chemistry 2019

View Article Online
DOI: 10.1039/C9DT00616H

Published on 28 March 2019. Downloaded on 3/29/2019 1:23:54 AM.

of inner orbitals that arise from the manganese *d* orbitals to the π* orbitals of the aromatic rings.

CO release properties

Because the synthesized compounds have a medium-dependent structure, the CO release activity was tested in both dichloromethane and acetonitrile solutions, by using an excitation wavelength of 380 ± 10 nm (λ_{380}), and the changes in the UV, IR and NMR spectra were monitored. Lower energy wavelengths were also employed however, as expected, show much slower CO release rates and for this reason not shown.

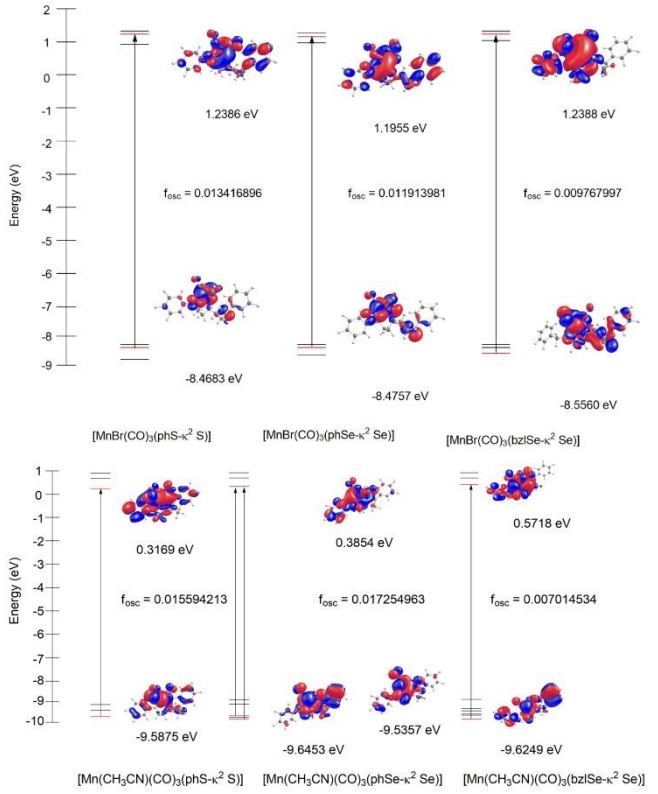

Figure 4. Calculated molecular orbitals for the first major transition in dichloromethane (top) and acetonitrile (bottom) at ωB97X-D3/def2 level of theory.

Table 4 Energies, oscillator strengths (f_{osc}) with main orbital contribution and type of orbitals involved in the first excitations at ωB97X-D3/def2 level of theory.

State	λ (nm)	f_{osc}	Type of transition
		[MnBr(CO)$_3$(phS-κ^2 S)]	
1	422.3	0.003610293	π (Mn-CO); p (Br) → π* (phenyl)
2	403.5	0.013416896	
		[MnBr(CO)$_3$(phSe-κ^2 Se)]	
1	418.2	0.001774086	π (Mn-CO); p (Br) → π* (phenyl)
2	400.6	0.011913981	
		[MnBr(CO)$_3$(bzlSe-κ^2 Se)]	
1	419.4	0.001882577	π (Mn-CO); p (Br) → π* (phenyl)
2	403.0	0.009767997	
		[Mn(CH$_3$CN)(CO)$_3$(phS-κ^2 S)]$^+$	
1	421.7	0.000968382	π (Mn-CO); π (phenyl) → π*
2	401.6	0.015594213	(phenyl)
		[Mn(CH$_3$CN)(CO)$_3$(phSe-κ^2 Se)]$^+$	
1	413.6	0.000718936	π (Mn-CO); π (phenyl) → π*
2	394.8	0.017254963	(phenyl)
		[Mn(CH$_3$CN)(CO)$_3$(bzl-κ^2 Se)]$^+$	
1	400.7	0.000860679	π (Mn-CO); π (phenyl) → π*
2	383.9	0.007014534	(phenyl)

In dichloromethane, in which the compounds retain the coordinated bromide, all compounds showed a steady decrease in the MLCT absorption bands at around 390 nm and the appearance of a new band at around 480 nm, with the formation of two isosbestic points during the processes, as seen in Figure 5 for **2** and Figures S19 and S20 for **1** and **3**. The decay in the MLCT band is due to the CO release process that lowers the concentration of the tricarbonyl species, forming photoproducts with a lower CO content, which shifts the MLCT bands to higher energies, as seen in the increase in absorbance at around 300 nm for compound **2** (Figure 5 for **2** and S19 and S20 for **1** and **3**).

Interestingly, a second lower energy band is formed at around 480 nm during the photoexcitation procedure, which at the time seemed unusual. However, mechanics studies by Kurz group[39,40] demonstrated that during the CO release of manganese carbonyl compounds a bis-carbonyl species with a solvent molecule that occupies the released CO is formed. In addition, because [Mn(CO)$_3$(tpa-κ^3 N)]$^+$ compound[27] binds the uncoordinated pyridine moiety after photoexcitation, it is feasible to postulate that this second band is associated with a [MnBr(CO)$_2$(L-κ^3 X)] species (in which L = phS, phSe or bzlSe and X = S or Se) for which the uncoordinated chalcogen moiety binds to the biscarbonyl species that is formed during the photoexcitation procedure. This photoproduct should have lower energy absorption values due to the presence of the second bonded chalcogen.

To verify that the biscarbonyl intermediate is formed in dichloromethane, the changes in the IR spectra of the products were also monitored. The analysis revealed a steady decrease in the three major CO stretching bands during the decomposition process. Concomitantly, formation of a new and lower frequency band at around 1800 cm^{-1} was observed. This CO stretching band is associated with antisymmetric stretching of the bis-carbonyl intermediate that is continuously formed during the decomposition process, as shown by Kurz's group.[39,40] Calculating the area under the curve after 840 s of exposure, 2.0, 2.2 and 2.2 equivalents of CO were released for **1-3** respectively, as seen in Figure 5 for **2** and S21 and S22 for **1** and **3**.

Unfortunately, the attribution of the intermediates by NMR spectroscopy was not possible due to rapid oxidation of the metal centre during the CO release procedure, which resulted in Mn^{II} species rapidly turning the solution paramagnetic, which gave broader peaks and hindered the collection of reliable results (Figure S23–S25).

By applying a pseud-first-order kinetics model to the decay in the UV spectra, it is possible to obtain the apparent CO release constants for **1–3**, which are, respectively, (1.82 ± 0.03) 10^{-3} s^{-1}, (7.76 ± 0.15) 10^{-3} s^{-1} and (7.87 ± 0.15) 10^{-3} s^{-1}.

Dalton Transactions Accepted Manuscript

View Article Online
DOI: 10.1039/C9DT00616H

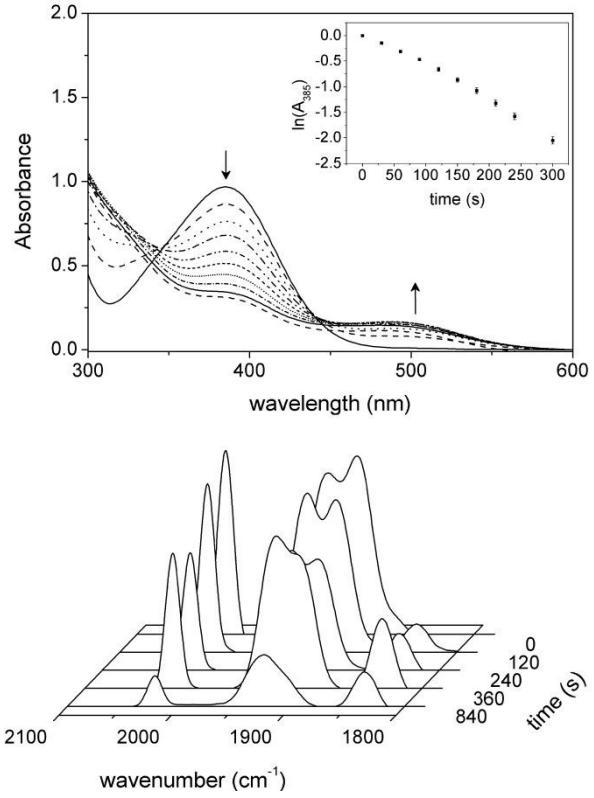

Figure 5 UV (top) and IR (bottom) spectral changes of **2** during excitation with a 380 ± 10 nm incident light in a dichloromethane solution.

Photoexcitation in acetonitrile with λ_{380} resulted in the formation of a brown to beige precipitate during the dissociation of CO by changing the colour of the solution from colourless to light yellow to deep yellow. This solid is related to the formation of Mn^{II} dimers after the dissociation of the first carbonyl group.[39,40] The precipitate formed during the irradiation inhibited the determination of the photoproducts in the required concentrations. This is due to the high degree of scattering of the irradiated light, which hindered the pseudo-first-order kinetic constants and made the results for the intermediates detected in KBr IR unreliable.

CO release in aqueous conditions and living cells

Having proven the complete dissociation of carbon monoxide from the compounds in the organic solvents, it was important to evaluate the ability of the compounds to release CO in physiological conditions. We could observe that the three compounds were able to release CO in a buffered aqueous solution (PBS, pH7.4), in response to COP-1, a fluorescent turn-on probe that selectively reacts with CO through a palladium-mediated carbonylation reaction.[41] In this assay, compound **2** was the most effective, because it was able to release 2x more CO than compounds **1** and **3** (Figure 6(a) and S26). Moreover, we could also detect increasing fluorescence levels, in a time dependent manner in HeLa cells (derived from cervical cancer) when incubated with the compounds for 15 min (**2** and **3**) and for 30min (**1**–**3**) in the presence of COP-1 [Figure 6 (c) and S27] relative to the control, which indicates increasing levels of CO release by compounds **1**–**3**.

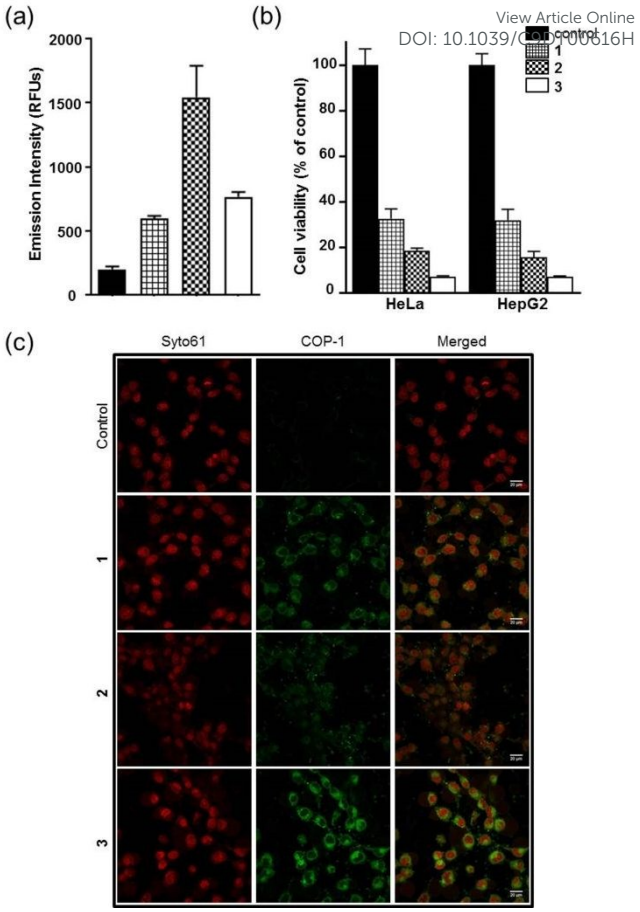

Figure 6. CO release in aqueous solution and cells. (a) Histogram representing the emission intensity (RFUs - relative fluorescent units) measured at 60min after incubation of 1 μM COP-1 (λ_{ex}=475 nm) with 150μM of compounds **1–3** in PBS pH 7.4 at 37 °C. The results correspond to Mean+ SEM of three independent experiments; (**b**) HeLa and HepG2 cell viability determined after 24h incubation with 150μM of **1–3.** Viability is represented as percentage of control (Mean + SEM of three independent experiments). (**c**) Representative confocal microscopy images of CO release in live HeLa cells untreated (control) and treated with 150 μM of **1**–**3** after 30min of incubation with COP-1. Left panel- nucleic acid staining with Syto61 (red), middle panel- COP-1 turn-on response to CO (green), right panel- merged channels.

Importantly, we could observe that the CO release is cytosolic and seems to be localized in the perinuclear region, which is in accordance to what was previously described for other CO-releasing molecules.[42] By considering that the aim of the use of CORMs is to selectively deliver CO to cells, as a therapeutic agent, we also addressed the cell viability of two different cancer cell lines, HeLa (cervical cancer) and HepG2 (liver cancer) after treatment with compounds **1**–**3**. Only 24h after treatment with 150μM of **1**–**3** less than 30% of cells are viable (Figure 6b). Although compound **3** is not the one that releases the most CO it seems to be the most potent against both cell lines because it is the one with lower IC50s (Figure S28). This effect may be due to the ability of compound **3** to release CO faster than the other compounds because 15min after incubation it shows a stronger intracellular fluorescence intensity relative to **1** and **2**, a tendency that is also visible after 30min of incubation (Figure 6b and S27). In addition, at 45min after incubation we can already see that the cells look altered, with abnormal nuclei and

Published on 28 March 2019. Downloaded on 3/29/2019 1:23:54 AM.

Dalton Transactions Accepted Manuscript

 This journal is © The Royal Society of Chemistry 2019

View Article Online
DOI: 10.1039/C9DT00616H

morphology, which is indicative of cell death (Figure S28). Thus, we believe that the effect of the compounds on cell death may occur within minutes after incubation, which is in accordance with the IR results that indicate a complete CO dissociation after 15min exposure.

Conclusions

In this study, three new manganese metal-carbonyl compounds were synthesized that contain heavy atoms in the first coordination sphere, namely sulfur and selenium. Even though the tridentate ligands where used, the MCCs synthesized had a κ^2-L X (X = S or Se) binding mode, detected by both the crystal structures and the asymmetry of the C-O stretching bands. The bonding analysis showed that the sulfur and selenium heavy-atom donors have unneglectable interactions with the carbonyls groups that make the CO *trans* to these moieties more stable in the ground state. Because the isolated compounds had an elusive binding mode, studies were conducted to determine the active species in solution, and the results show that in acetonitrile solution only the substitution of the bromide by an acetonitrile molecule occurs, without formation of κ^3-L. Moreover, the photoactivity of compounds **1–3**, showed that the CO release activity was solvent dependent. In dichloromethane it was found that the pseudo-first-order constants follow the trend k3 ≈ k2 > k1, which clearly show that the use of heavier atoms in the first coordination sphere can considerably increase the CO release rate, even without the expected bathochromic shift of the MLCT bands, which could prove useful in reducing the exposure time of the patients to UV-A light. This increase in the CO release rate is directly related to the dissociative populated excited states. In this regard more measures are required to fully understand the nature of these states, and how the increase in the SOC of the ligand increases the CO release rate, contrary to what is known of Mn and Re compounds, which in this case decreases the CO release.

Experimental

General

^{1}H NMR spectra were obtained at 400 MHz with a Varian AS-400 NMR spectrometer. Spectra were recorded in $CDCl_3$ solutions. Chemical shifts are referenced to the solvent peak of $CDCl_3$ or tetramethylsilane as the external reference. Data are reported as follows: chemical shift (δ), multiplicity, coupling constant (J) and integration intensity. ^{13}C NMR spectra were obtained at 100 MHz with a Varian AS-400 NMR spectrometer. Spectra were recorded in $CDCl_3$ solutions. Chemical shifts are referenced to the solvent peak of $CDCl_3$. ^{77}Se NMR spectra were obtained at 38.14 MHz with a Bruker AC-200 NMR spectrometer. Spectra were recorded in $CDCl_3$ solutions. Chemical shifts are referenced to diphenyl diselenide as the external reference (463.15 ppm). Abbreviations to denote the multiplicity of a particular signal are: s (singlet), d (doublet), t (triplet) and m (multiplet). High-resolution mass spectra were recorded with a Bruker micrOTOF-Q II APPI mass spectrometer equipped with an automatic syringe pump for sample injection. Infrared spectra were recorded with a Bruker Optics Alpha benchtop FT-IR spectrometer. The melting points were determined in a Microquimica MQRPF-301 digital model equipment with heating plate. Column chromatography was performed with silica gel (230-400 mesh). Thin layer chromatography was performed with Merck Silica Gel GF254, 0.25 mm thickness. Samples were visualized either under ultraviolet light or stained with iodine vapor and acidic vanillin. Reactions under inert atmosphere were conducted in flame-dried or oven-dried glassware equipped with tightly fitted rubber septa and under a positive atmosphere of dry argon. Reagents and solvents were handled by using standard syringe techniques. Temperatures were maintained by use of a mineral oil bath with a heating and stirring plate.
The IR, ^{1}H, ^{13}C and ^{77}Se NMR spectra can be found in the Supplementary Information.

Synthesis of ligands containing sulfur and selenium (1'–3')

Ethanol (5.0 ml) and the appropriate diorganoyl dichalcogenide (3.0 mmol) were placed in a 25 mL round-bottomed flask under an argon atmosphere. To the stirred reaction mixture, $NaBH_4$ (6.0 mmol) was added in small portions. After the complete evolution of gas, bis(2-chloroethyl)amine hydrochloride (2.0 mmol) dissolved in ethanol was added dropwise. The reaction mixture was then heated at 70 °C for 18 h then allowed to cool to room temperature. The solvent was removed by evaporation under reduced pressured. The crude mixture was dissolved in ethyl acetate (30 mL) and extracted with water (3 x 10 mL). The combined organic phase was washed with brine, dried with anhydrous $MgSO_4$, and concentrated under reduced pressure. The crude material was purified by column chromatography (hexane/ethyl acetate 7:3).

Bis(2-(phenylthio)ethyl)amine (1'). Yellow oil. Yield 288 mg; 289.46 g mol^{-1}; 50%.^{1}H NMR (400 MHz, CDCl3): δ = 7.34 (d, J = 4.0 Hz, 3H), 7.25 (t, J = 8.0 Hz, 4H), 7.19–7.15 (m, 2H), 3.03 (t, J = 8.0 Hz, 4H), 2.80 (t, J = 8.0 Hz, 4H), 1.88 (s, 1H) ppm. ^{13}C NMR (100 MHz, $CDCl_3$): δ = 135.7 (C), 129.8 (CH), 128.9 (CH), 126.3 (CH), 47.8 (CH_2), 34.2 (CH_2) ppm. Selected IR frequencies (KBr): 3300.3, 3057.6, 2920.9, 2829.1, 1945.9, 1640.0, 1582.8, 1478.8, 1438.0, 1121.9, 1024.0, 738.4, 691.5, 475.3 cm^{-1}.[32]

Bis(2-(phenylselanyl)ethyl)amine (2'). Off-white solid. Yield: 514 mg; 383.28 g mol^{-1}; 71%. M.p. 110-112 °C (lit. 106 °C). ^{1}H NMR (400 MHz, $CDCl_3$): δ = 7.51–7.48 (m, 3H), 7.27–7.22 (m, 5H), 3.00 (t, J = 6.6 Hz, 4H), 2.85 (t, J = 6.6 Hz, 4H), 1.77 (s, 1H) ppm. ^{13}C NMR (100 MHz, $CDCl_3$): δ = 133.1 (CH), 129.7 (C), 129.2 (CH), 127.1 (CH), 48.6 (CH_2), 28.6 (CH_2) ppm. ^{77}Se NMR (38.14 MHz, $CDCl_3$): δ = 266.21 ppm. Selected IR frequencies (KBr): 3430.7, 3051.3, 2812.7, 1947.9, 1576.6, 1476.7, 1433.88, 1144.2, 1019.8, 732.2, 693.5 cm^{-1}.[32]

Bis(2-(benzylselanyl)ethyl)amine (3'). Yellow oil. Yield: 658 mg; 411.33 g mol^{-1}; 80%. ^{1}H NMR (400 MHz, $CDCl_3$): δ = 7.31–7.18 (m, 9H), 3.77 (s, 4H), 2.73 (t, J = 6.6 Hz, 4H), 2.60 (t, J = 6.6 Hz, 4H), 1.66 (br. s, 1H) ppm. ^{13}C NMR (100 MHz, $CDCl_3$): δ = 139.4

Published on 28 March 2019. Downloaded on 3/29/2019 1:23:54 AM.

Dalton Transactions Accepted Manuscript

View Article Online
DOI: 10.1039/C9DT00616H

Published on 28 March 2019. Downloaded on 3/29/2019 1:23:54 AM.

(C), 128.9 (CH), 128.6 (CH), 126.8 (CH), 48.7 (CH_2), 27.1 (CH_2), 24.6 (CH_2) ppm. ^{77}Se NMR (38.14 MHz, $CDCl_3$): δ = 255.79 ppm. HRMS- (APPI): m/z calcd. for $[C_{18}H_{23}NSe_2]^+$ $[M+nH]^+$ 414.0237; found 414.0236.

Synthesis of Mn compounds that contain sulfur and selenium 1–3

For the preparation of the carbonyl compounds, a solution of the appropriate organochalcogen ligand (0.25 mmol) was solubilized in a mixture of dichloromethane (1 mL) and diethyl ether (4 mL). The resulting solution was degassed by applying two freeze-pump-thaw cycles. The manganese precursor $[MnBr(CO)_5]$ (0.25 mmol) was added to a frozen solution of the ligands, thaw degassed three times and then kept under agitation until the mixture reached room temperature. The mixture was then heated to reflux under an inert atmosphere and dim light conditions overnight to give brown solutions. To the cooled mixture, hexane (10 mL) was added and kept at 25°C for two days to give dark yellow crystals suitable for X-ray analysis.

$[MnBr(CO)_3(phS-\kappa^2 S)]$ (1). Dark yellow solid. Yield: 742 mg; 511.35 g mol^{-1}; 72%. Selected IR frequencies (ATR): 2020 (s, ν_{CO}), 1933 (s, ν_{CO}), 1912 (s, ν_{CO}), 1610-1433 (w, ν_{ar}), 757 (m, δ_{ar}), 633 (m, δ_{ar}) cm^{-1}. Selected electronic absorption wavelengths (CH_2Cl_2, λ_{max} in nm) and their respective ε values (L mol^{-1} cm^{-1}): 385 (2757). Found and calculated elemental analysis ($C_{19}H_{19}NO_3S_2BrMn$): C, 44.81 (44.89); H, 3.75 (3.77); N, 2.87 (2.76).

$[MnBr(CO)_3(phSe-\kappa^2 Se)]$ (2). Dark yellow solid. Yield: 742 mg; 605.14 g mol^{-1}; 76%. Selected IR frequencies (ATR): 2015 (s, ν_{CO}), 1919 (s, ν_{CO}), 1896 (s, ν_{CO}), 1605-1435 (w, ν_{ar}), 760 (m, δ_{ar}), 630 (m, δ_{ar}) cm^{-1}. Selected electronic absorption wavelengths (CH_2Cl_2, λ_{max} in nm) and their respective ε values (L mol^{-1} cm^{-1}): 385 (2235). Found and calculated elemental analysis ($C_{19}H_{19}NO_3Se_2BrMn$): C, 39.42 (39,37); H, 4.83 (4.72); N, 1.77 (2.81).

$[MnBr(CO)_3(bzlSe-\kappa^2 Se)]$ (3). Dark yellow solid. Yield: 742 mg; 633.20 g mol^{-1}; 68%. Selected IR frequencies (ATR): 2015 (s, ν_{CO}), 1927 (s, ν_{CO}), 1908 (s, ν_{CO}), 1602-1430 (w, ν_{ar}), 755 (m, δ_{ar}), 627 (m, δ_{ar}) cm^{-1}. Selected electronic absorption wavelengths (CH_2Cl_2, λ_{max} in nm) and their respective ε values (L mol^{-1} cm^{-1}): 388 (2014). Found and calculated elemental analysis ($C_{21}H_{23}NO_3Se_2BrMn$): C, 40.25 (40.02); H, 3.56 (3.68); N, 2.11 (2.22).

Single-Crystal X-ray Structure Determinations

Crystallographic analyses were carried out with a Bruker APEX II DUO diffractometer with graphite-monochromated Mo-Kα radiation (l = 0.71069 Å), at 200(2) K. Images were recorded by using the ϕ and ω scan method. Semi-empirical absorption correction[43] was also applied to all measured intensities with maximum and minimum transmission factors shown in Table S1. The structures were solved by direct methods and refined by the full-matrix least-squares on F^2.[44] H atoms attached to C atoms were placed at their idealized positions, with C–H distances and U_{eq} values taken from the default settings of the refinement program. Hydrogen atoms of the amine groups were found from the Fourier difference map and treated as free atoms. ORTEP plots were drawn with the PLATON program.[45] Selected crystallographic information are summarized in the Supplementary Information file. Full crystallographic tables (including structure factors) have been deposited with the Cambridge Crystallographic Data Centre as supplementary publication numbers CCDC 1894674, 1894675 and 1894677. These data can be obtained free of charge from the Cambridge Crystallographic Data Centre at www.ccdc.cam.ac.uk.

Computational Methods

Geometries for all compounds were obtained by using DFT[45,46] with the BP86[47] exchange correlation functional and Grimme's D3BJ dispersion correction[48] along with the def2-TZVP basis set[49] as implemented in the Orca package, version 3.0.2.[50] Structures were confirmed as minima by the absence of imaginary eigenvalues in the generalized Hessian matrix.

GKS-EDA[51] as implemented in GAMESS-US 2012,[52] was performed with the BP86 functional[47] by using Grimme's D3 correction[48] and the def2-SVP basis set.[53] The Boys and Bernardi approach[54] was used to correct for basis set superposition errors. In all cases a CO ligand was considered as a neutral fragment whereas the remainder of the molecule was the second fragment without residual charges. The GKS-EDA scheme decomposes the instantaneous interaction energy (ΔE^{int}) into the sum of six physical meaningful terms: electrostatic (ΔE^{elstat}), exchange (ΔE^{exch}), repulsion (ΔE^{rep}), polarization (ΔE^{pol}), dispersion (ΔE^{disp}) and correlation (ΔE^{corr}). Natural bond orbital analysis[55] was also performed in conjunction with GKS-EDA to support the bonding analysis of CO groups.

For the frequencies and singlet excitations, geometries for all compounds were obtained by using DFT[45,46] with the ωB97X-D3[56] exchange correlation functional along with the def2-SVP basis[53] for carbon and hydrogen atoms, the def2-TZVP(-f) basis set for carbon and nitrogen in the first coordination sphere, and oxygen atoms, and the def2-TZVP basis for the heavy atoms S, Se, Br and Mn,[53] as implemented in the Orca package, version 4.0.1.[57] To speed up the calculations, the RIJCOSX approximation was used.[58] Structures were confirmed as minima by the absence of imaginary eigenvalues in the Hessian matrix. The resulting structures were then optimized by taking into account solvation effects by using the SMD solvation model,[59] as implemented in the Orca package, by using the appropriate solvent. The excited state wavefunctions and the transition oscillator strengths within TDA approximation were calculated using the TD-DFT calculations,[60] in which the first forty roots were considered on the same basis as before.

Investigation in living cells

Cell culture. HepG2 (a human hepatoma cell line) and HeLa cells (derived from cervical cancer cells) were maintained in a humidified incubator at 37 °C under 5% CO_2 and grown byh using 1x D-MEM ((Invitrogen, Life Technologies) supplemented with 10% heat-inactivated fetal bovine serum (FBS) (Gibco, Life Technologies), 1x MEM NEAA (Gibco, Life Technologies), 1x GlutaMAX (Gibco, Life Technologies), 200 units mL-1 penicillin

Dalton Transactions Accepted Manuscript

 This journal is © The Royal Society of Chemistry 2019

Published on 28 March 2019. Downloaded on 3/29/2019 1:23:54 AM.

and 200 µg mL-1 streptomycin (Gibco, Life Technologies) and 10 mM HEPES (Gibco, Life Technologies).

Cell viability assay. To determine cell viability a CellTiter Blue assay was performed. For this purpose 10.000 cells per well were seeded in 96 well-plates and 24h later were treated with 1, 5, 10, 25, 50, 100 and 150µM of either phS, phSe and bzlSe. After 24h or 48h after treatment, the cells incubated with CellTiter blue for 1h 30min at 37**°**C after which the viability was determined by measuring the Emission Intensity in RFUs with an Infinite M200 plate reader.

CO release in aqueous solution. The quantification of the CO release promoted by the compounds in aqueous solution was determined by COP-1 fluorescence on different time points (0, 10, 20, 30, 40, 50, 60, 70, 80 and 90min) and different wave lengths (490 to 610nm). Hence, 150 µM of the compounds in PBS, were mixed with a 1 µM solution of COP-1 (synthesized according to the literature)[31] and COP-1 fluorescence was measured using an Infinite M200 plate reader. A solution of COP-1 with PBS was used as a negative control

CO release in cells. A total of $3x10^4$ HeLa cells per well were seeded in a 8-chambered Ibidi cell plate. Thirty minutes before measuring CO release, the cells were incubated with a 1:2000 dilution on Syto61 (Lyfe Technologies) for nuclear staining. After the 30min incubation time, the cells were washed and incubated with 1 µM of COP-1 and 150 µM of the compounds, in medium with reduced phenol red, and were immediately observed by using a Zeiss LSM 710 confocal Laser Point-Scanning Microscope with a 40X oil objective lens and a numerical aperture of 1.3. Throughout the experiment the cells were maintained at 37 **°**C. COP-1 was excited by using an Argon Laser with wavelength of 488 nm, whereas Syto61 was excited by using a DPSS 561-10 laser (561nm). COP-1 was read at green ("em 500-550 nm) and Syto61 in red ("em 570-640 nm). Mean of total fluorescence intensity of treated and untreated cells were determined with the help of ImageJ software. Statistically significant differences were tested with a Mann Whitney test. Data are presented in the graphs as mean of total fluorescent intensity ± SEM.

Conflicts of interest

There are no conflicts to declare.

Acknowledgements

Funded under the Brazilian governmental agencies CNPq (PVE - 400210/2014-2), CNPq, and CERSusChem GSK/FAPESP (grant 2014/50249-8) grants for A. Neves, A. L. Braga, A. L. Amorim and R. A. Peralta, CAPES (Finance Code 001). We also thank the FAPESC, EU Horizon 2020 programme, Marie Skłodowska-Curie ITN GA no. 675007 and TWINN-2017 ACORN, GA no. 807281, the Royal Society (UF110046 and URF\R\180019 to G.J.L.B.), FCT Portugal (iFCT IF/00624/2015 to G.J.L.B. and PhD studentship SFRH/BD/115932/2016 to A.G.), and an ERC StG (GA no. 676832) for funding. The authors thank Prof. Chris Chang for providing COP-1, and Dr Vikki Cantrill for her help with the editing of this manuscript. The authors also acknowledge CEBIME for the HRMS analysis.

View Article Online
DOI: 10.1039/C9DT00616H

Notes and references

1 H. P. Kim, S. W. Ryter and A. M. Choi, *Annu. Rev. Pharmacol. Toxicol.*, 2006, **46**, 411-449.
2 J. M. Fukuto, S. J. Carrington, D. J. Tantillo, J. G. Harrison, L. J. Ignarro, B. A. Freeman, A. Chen, and D. A. Wink, *Chem. Res. Toxicol.*, 2012, **25**, 769-793.
3 R. Foresti, M. G. Bani-Hani, and R. Motterlini, *Intensive Care Med.*, 2008, **34**, 649-658.
4 S. García-Gallego and G. J. L. Bernardes, *Angew. Chem. Int. Ed.*, 2014, **53**, 9712-9721.
5 R. Motterlini, B. E. Mann and R. Foresti, *Expert Opin. Invest. Drugs*, 2005, **14**, 1305-1318.
6 R. Motterlini and L. E. Otterbein, *Nat. Rev. Drug Discovery*, 2010, **9**, 728-743.
7 B. E. Mann, *Organometallics*, 2012, **31**, 5728-5735.
8 C. C. Romão, W. A. Blättler, J. D. Seixas and G. J. L. Bernardes, *Chem. Soc. Rev.*, 2012, **41**, 3571-3583.
9 U. Schatzschneider, *Br. J. Pharmacol.* 2015, **172**, 1638-1650.
10 R. D. Rimmer, A. E. Pierri and P. C. Ford, *Coord. Chem. Rev.*, 2012, **256**, 1509–1519.
11 X. Ji, C. Zhou, K. Ji, R. E. Aghoghovbia, V. Chittavong, B. Ke, B. Wang, *Angew. Chem. Int. Ed. Engl.* **2016**, 55, 15846-15851.
12 L. A. P. Antony, T. Slanina, P. Sebej, T. Solomek and P. Klán, *Org. Lett.* 2013, **15**, 4552-4555.
13 M. Popova, T. Soboleva, A. M. Arif, L. M. Berreau, *RSC Adv.* **2017**, 7, 21997–22007.
14 S. N. Anderson, J. M. Richards, H. J. Esquer, A. D. Benninghoff, A. M. Arif, L. M. Berreau, *ChemistryOpen*, **2015**, 4, 590-594.
15 E. Palao, T. Slanina, L. Muchova, T. Solomek, L. Vitek, P. Klan, *J. Am. Chem. Soc.*, **2016** ,138, 126–133.
16 T. I. Ayudhya, P. J. Pellechia and N. N. Dingra, *Dalton Trans.*, **2018**, 47, 538-543.
17 D. Wang, E. Viennois, K. Ji, K. Damera, A. Draganov, Y. Zheng, C. Dai, D. Merlin and B. Wang, *Chem. Commun.*, **2014**, 50, 15890–15893.
18 Y. Zheng, X. Ji, B. Yu, K. Ji, D. Gallo, E. Csizmadia, M. Zhu, M. R. Choudhury, L. K. C. De La Cruz, V. Chittavong, Z. Pan, Z. Yuan, L. E. Otterbein, B. Wang, *Nat. Chem.*, **2018**, 10, 787–794.
19 T. R. Johnson, B. E. Mann, I. P. Teasdale, H. Adams, R. Foresti, C. J. Green and R. Motterlini, *Dalton Trans,* 2007, **15**, 1500–1508.
20 R. Kretschemer, G. Guessner, H. Görls, S. H. Heinemann and M. J. Westerhausen, *Inorg. Biochem.*, 2011, **105**, 6-9.
21 F. Zobi, O. Blacque, R. A. Jacobs, M. C. Schaub and A. Y. Bogdanova, *Dalton Trans.*, 2012, **41**, 370-378.
22 A. R. Marques, L. Kromer, D. J. Gallo, N. Penacho, S. S. Rodrigues, J. D. Seixas, G. J. L. Bernardes, P. M. Reis, S. L. Otterbein, R. A. Ruggieri, A. S. G. Gonçalves, A. M. L. Gonçalves, M. N. D. Matos, I. Bento, L. E. Otterbein, W. A. Blättler and C. C. Romão, *Organometallics*, 2012, **31**, 5810-5822.
23 U. Schatzschneider, *Inorg. Chim. Acta*, 2011, **374**, 19-23.
24 A. M. Mansour, A. Friedrich, *Inorg. Chem. Front.*, 2017, **4**, 1517-1524.
25 J. Jimenez, I. Chakraborty, S. J. Carrington, P. K. Mascharak, *Dalton Trans.*, 2016, **45**, 13204-13213.
26 Z. Li, A. E. Pierri, P. Huang, G. Wu, A. V. Iretskii, P. C. Ford, *Inorg. Chem.*, **2017**, 56, 6094-6104.
27 C. Nagel, S. McLean, R. K. Poole, H. Braunschweig, T. Kramer and U. Schatzschneider, *Dalton Trans.*, 2014, **43**, 9986-9997.
28 J. Jimenez, I. Chakraborty, A. Dominguez, J. Martinez-Gonzalez, W. M. C. Sameera and P. K. Mascharak, *Inorg. Chem.*, 2018, **57**, 1766-1773.
29 S. J. Carrington, I. Chakraborty and P. K. Mascharak, *Dalton Trans.*, 2015, **44**, 13828-13834.

Dalton Transactions Accepted Manuscript

30 E. Kottelat, A. Ruggi, F. Zobi, *Dalton Trans.*, 2016, **45,** 6920–6927.
31 H. C. Braga, C. A. M. Salla, I. H. Bechtold, A. J. Bortoluzzi, B. de Souza and H. Gallardo, *Dyes Pigments*, 2017, **117**, 149-156.
32 S. Kumar, G. K. Rao, A. Kumar, M. P. Singh, A. K. Singh, *Dalton Trans.*, 2013, **42**, 16939–16948.
33 R. Mede, J. Traber, M. Klein, H. Görls, G. Gessner, P. Hoffmann, M. Schmitt, J. Popp, S. H. Heinemann, U. Neugebauer and M. Westerhausen, *Dalton Trans.*, 2017, **46**, 1684-1693.
34 M. A. Gonzalez, S. J. Carrington, N. L. Fry, J. L. Martinez and P. K. Mascharak, *Inorg. Chem.*, 2012, **51**, 11930-11940.
35 F. Mohr, J. Niesel, U. Schatzschneider and C. W. Z. Lehmann, *Anorg. Allg. Chem.*, 2011, **638**, 543-546.
36 M. A. Gonzalez, S. J. Carrington, N. L. Fry, J. L. Martinez and P. K. Mascharak, *Inorg. Chem.*, 2012, **51**, 11930-11940.
37 I. Chakraborty, S. J. Carrington and P. K. Mascharak, *Acc. Chem. Res.*, 2014, **47**, 2603-2611.
38 R. N. Pickens, B. J. Neyhouse, D. T. Reed, S. T. Ashton and J. K. White, *Inorg. Chem.* 2018, **57**, 11616-11625.
39 H-M. Berends and P. Kurz, *Inorg. Chim. Acta.*, 2011, **380**, 141-147.
40 U. Sachs, G. Schaper, D. Winkler, D. Kratzert and P. Kurz, *Dalton Trans.*, 2016, **45**, 17464-17473.
41 B. W. Michel, A. R. Lippert and C. J. Chang, *J. Am. Chem. Soc.*, 2012, **134**, 15668-15671.
42 M. Chaves-Ferreira, I. S. Albuquerque, D. Matak-Vinkovic, A. C. Coelho, S. M. Carvalho, L. M. Saraiva, C. C. Romão and G. J. L. Bernardes, *Angew. Chem. Int. Ed.*, 2015, **54**, 1172 -1175.
43 APEX2, SAINT and SADABS. version 2011.8-0; Bruker AXS Inc., Madison, Wisconsin, USA.
44 G. M. Sheldrick, *Acta Cryst.*, 2015, **C71**, 3-8.
45 P. Hohenberg and W. Kohn, *Phys. Rev.*, 1964, **136**, B864-B871.
46 W. Kohn and L. J. Sham, *Phys. Rev.* 1965, **140**, A1133-A1138.
47 J. P. Perdew, *Phys. Rev. B*, 1986, **33**, 8822-8824.
48 S. Grimme, J. Antony, S. Ehrlich and H. Krieg, *J. Chem. Phys.*, 2010, **132**, 154104.
49 K. Eichkorn, F. Weigend, O. Treutler and R. Ahlrichs, *Theor. Chem. Acc.*, 1997, **97**, 119-124.
50 F. Neese, *WIREs Comput. Mol. Sci.* 2012, **2**, 73-78.
51 P. Su, Z. Jiang, Z. Chen and W. Wu, *J. Phys. Chem. A,* 2014, **118**, 2531-2542.
52 M. W. Schmidt, K. K. Baldridge, J. A. Boatz, S. T. Elbert, M. S. Gordon, J. H. Jensen, S. Koseki, N. Matsunaga, K. A. Nguyen, S. Su, T. L. Windus, M. Dupuis and J. A. Montgomery, *J. Comput. Chem.*, 1993, **14**, 1347-1363.
53 K. Eichkorn, O. Treutler, H. Öhm, M. Häser and R. Ahlrichs, *Chem. Phys. Lett.*, 1995, **240**, 283-290.
54 S. F. Boys and F. Bernardi, *Mol. Phys.* 2002, **100**, 65-73.
55 E. D. Glendening, C. R. Landis and F. Weinhold, *WIREs Comput. Mol. Sci.*, 2012, **2**, 1-42.
56 J. -D. Chai, M. Head-Gordon, *J. Chem. Phys.*, 2008, **128**, 084106.
57 F. Neese, *WIREs Comput. Mol. Sci.* 2018, **8**, e1327.
58 T. Petrenko, S. Kossmann and F. Neese, *J. Chem. Phys.*, 2011, **134**, 054116.
59 A. V. Manerich, C. J. Cramer and D. G. Truhlar, *J. Phys. Chem. B*, 2009, **113**, 6378.
60 F. Neese and G. Olbrich, *Chem. Phys. Lett.*, 2002, **362**, 170-178.

View Article Online
DOI: 10.1039/C9DT00810H

Published on 28 March 2019. Downloaded on 3/29/2019 1:23:54 AM.

Dalton Transactions Accepted Manuscript

This journal is © The Royal Society of Chemistry 2019